PHOTONICS Research

Ultrapure and highly efficient green light emitting devices based on ligand-modified $CsPbBr_3$ quantum dots

Dongdong Yan, Shuangyi Zhao, Huaxin Wang, and Zhigang Zang*

Key Laboratory of Optoelectronic Technology & Systems (Ministry of Education), Chongqing University, Chongqing 400044, China
**Corresponding author: zangzg@cqu.edu.cn*

Received 2 March 2020; revised 12 April 2020; accepted 18 April 2020; posted 20 April 2020 (Doc. ID 391703); published 3 June 2020

All inorganic $CsPbBr_3$ perovskite quantum dots (QDs) have been recognized as promising optical materials to fabricate green light emission devices because of their excellent optical performance. However, regular $CsPbBr_3$ QDs with an oleic acid (OA) ligand show poor stability, which limits their practical application. We replaced the OA ligand in $CsPbBr_3$ QDs with a 2-hexyldecanoic acid (DA) ligand and, in the synthesis, found that the new material has better optical properties than regular $CsPbBr_3$ QDs ($CsPbBr_3$-OA QDs). Due to the strong binding energy between the DA ligand and QDs, the ligand-modified $CsPbBr_3$ QDs ($CsPbBr_3$-DA QDs) show a high photoluminescence quantum yield (PLQY) of 96%, while the PLQY of $CsPbBr_3$-OA QDs is 84%. Subsequently, the $CsPbBr_3$ QDs coated on the blue light-emitting diode (LED) chips as green phosphors are demonstrated. The color conversion from blue to pure green is achieved by adding the $CsPbBr_3$-OA QDs solution up to 60 μL, while the pure green emission devices only need 18 μL $CsPbBr_3$-DA QDs solution under the same concentration. The ultrapure, highly efficient green light-emitting devices based on $CsPbBr_3$-DA QDs exhibit a luminous efficiency of 43.6 lm/W with a CIE (0.2086, 0.7635) under a 15.3 mA driving current. In addition, the green emission wavelength of the devices based on $CsPbBr_3$-DA QDs almost has no shift, even under a high injection current. These results highlight the promise of DA ligand-modified $CsPbBr_3$ QDs for light-emitting devices and enrich the application field of ligand-modified $CsPbBr_3$ QDs.

https://doi.org/10.1364/PRJ.391703

1. INTRODUCTION

Light-emitting diodes (LEDs) have been recognized as efficient solid-state lighting sources and are widely used in the photoelectric field due to advantages such as high efficiency, a long lifetime, and a low power requirement. To improve the color-rendering index (Ra > 80) of white LEDs, the green and red contents in the spectra should be enlarged. In particular, the green light source is considered to have an important role in white LEDs [1]. Unfortunately, it is difficult to achieve high-efficiency green LEDs because of the well-known "green gap" problem [2–8]. In general, compared to the blue GaN-based LEDs counterparts, green GaN-based LEDs show much lower external quantum efficiency (EQE) and a stronger efficiency drop effect. To achieve efficient green LEDs, various efforts have been explored. For example, Saito *et al.* reported enhanced LEDs using the active layer consisting of the AlGaN interlayer and InGaN quantum well [9]. In addition, a series of studies about rare-earth-doped green phosphor materials also have been proposed [10–13]. However, phosphor-based green LEDs still impede the practical application due to their poor monochromaticity and wide bandwidth [14,15]. Therefore, it is still necessary to develop high-efficiency green emission materials with good monochromaticity and a narrow bandwidth.

Recently, all-inorganic perovskite $CsPbX_3$ (X = Cl, Br, I) quantum dots (QDs) have emerged as a new class of optical materials that have great potential for applications in the photoelectric field [16–22], because of their high optical gain, narrow emission width, and high photoluminescence quantum yield (i.e., PLQY above 85%) [23–27]. Moreover, recent reports using novel strategies on $CsPbX_3$ QDs have enriched the applications. Ooi *et al.* [28] demonstrated the potential application of $CsPbBr_3$ QDs for visible light communication. Their group also explored a high-speed UV color-converting photodetector based on $CsPbBr_3$ [29]. Zeng's group demonstrated that $CsPbX_3$ QDs exhibit promising materials for high-definition QD displays and lighting devices [30]. Among the family of $CsPbX_3$ QDs, $CsPbBr_3$ QDs have been regarded as particularly promising for LEDs [31,32]. To date, much effort has been devoted to achieving green light emission using GaN-based LEDs that convert their blue or near-ultraviolet (UV) emission into green light via an interaction with inorganic $CsPbBr_3$

perovskite QDs [22,33]. However, the reported $CsPbBr_3$ QDs capped with long alkyl ligands such as oleic acid (OA) and oleylamine (OAM) synthesized by a hot-injection method exhibit unsatisfactory stabilities, which hinder their practical application in LEDs [34,35]. To improve the performance of LEDs based on $CsPbBr_3$ QDs, some useful strategies have been proposed. The EQE of green $CsPbBr_3$ perovskite QDs-based LEDs obviously could be enhanced through surface ligand engineering [36] and surface treatments [37,38]. Among those strategies, ligand modification of $CsPbBr_3$ QDs also has been demonstrated to be an effective method to improve luminescent performance [39]. Replacing a long ligand (for example, an OA ligand) with a shorter ligand without degrading or destabilizing the perovskite structure is the key challenge for a $CsPbBr_3$ QDs application. As presented in our previous report, we prepared high-quality $CsPbBr_3$ QDs using a 2-hexyldecanoic acid (DA) with two short branched chains to replace an OA ligand with long chains in the synthesis process. During the process, the $CsPbBr_3$ QDs with a DA ligand ($CsPbBr_3$-DA QDs) exhibited more excellent stability and optical properties than the regular $CsPbBr_3$ QDs with an OA ligand ($CsPbBr_3$-OA QDs) [40]. However, to the best of our knowledge, there has been no report about $CsPbBr_3$-DA QDs used as phosphors for green light emission devices. In this study, we aim to investigate the potential of modified $CsPbBr_3$ QDs in light emission devices.

We synthesized high-performance $CsPbBr_3$ QDs by using a shorter 2-hexyldecanoic acid (DA) ligand to replace an OA ligand for $CsPbBr_3$ QDs. The ligand-modified $CsPbBr_3$ QDs show a high PLQY of 96%, which were used as green phosphors for high-performance light emission devices. As a result, ultrapure and highly efficient green light-emitting devices based on $CsPbBr_3$-DA QDs exhibit a luminous efficiency of 43.6 lm/W with a CIE (0.2086, 0.7635) under a 15.3 mA driving current. Furthermore, the green light-emitting devices based on $CsPbBr_3$-DA QDs also have a more stable green emission than the devices based on $CsPbBr_3$-OA QDs under various driving currents. Thus, we believe that ligand modification is an effective way to improve the performance of light emission devices.

2. EXPERIMENT

Chemicals and reagents: Cs_2CO_3 (99.9%) and $PbBr_2$ (99.9%) were purchased from Xi'an Polymer Light Technology Corp. OAm (>90%, Adamas), OA (>90%, Adamas), DA (>98%, TCI), octadecene (ODE, >90%, Adamas) were used without further purification.

Synthesis of $CsPbBr_3$-OA QDs and $CsPbBr_3$-DA QDs: ODE (4 mL), Cs_2CO_3 (81.5 mg), and 0.5 mL OA were loaded into the 100 mL three-neck flask 1 with stirring; $PbBr_2$ (0.188 mmol) and ODE (5 mL) were loaded into another 100 mL three-neck flask 2 with stirring. The two flasks were degassed at 120°C for 1 h under vacuum and nitrogen flow, then OA (0.5 mL) and OAm (0.5 mL) were quickly injected into flask 2, and the temperature rose to 150°C in 2 min in a nitrogen environment. A 0.4 mL of Cs-oleate solution was quickly injected. After 5 s, the crude reaction solution was cooled by the ice water bath. The synthesis of $CsPbBr_3$-DA QDs was similar to that of $CsPbBr_3$-OA QDs, except that the OA ligands were replaced by DA ligands.

Fabrication of $CsPbBr_3$ QDs films: The QDs films were fabricated by spin-coating 400 μL of 10 mg/mL solution of $CsPbBr_3$ QDs (in n-octane) onto glass substrates (1.5 cm × 1.5 cm) in air. The speed of spin-coating was 2500 r/min (15 s). Thus, the ~300 nm thick $CsPbBr_3$-OA QDs films could be obtained. The $CsPbBr_3$-DA QDs films with the same thickness were also fabricated by this method.

Green LEDs fabrication: First, the 10 mg $CsPbBr_3$ QDs were dissolved in 1 mL n-octane to obtain a homogenous solution. Then, the mixture was put in a vacuum chamber to get rid of the bubbles inside. Finally, the 6 μL $CsPbBr_3$ QDs solution was directly dropping-coated into the LED groove using a pipettor. Then, the LED was baked at 50°C to volatilize n-octane and to form the QDs layer. The thickness of the layer created by 6 μL QDs solution was estimated to be about 40 nm, and also the film thickness has a linear relationship with the dropped solution.

Materials and devices characterization: The X-ray diffraction (XRD) analysis was performed on XRD-6100 (Shimadzu, Japan). The purified samples were redispersed in 0.5 mL n-octane and then dropped on 0.8 cm by 0.8 cm glass substrates followed by solvent evaporation. The transmission electron microscopy (TEM) and high-resolution TEM (HRTEM) images were performed using an electron microscope (Libra 200 FE, Carl Zeiss AG, Oberkochen, Germany). The absorption spectra were measured by a UV-vis spectrophotometer (UV-2100, Shimadzu, Kyoto, Japan). Samples with the same thickness were prepared by dropping the QDs solution (300 μL of 10 mg/mL solution of $CsPbBr_3$ QDs) onto glass substrates. The photoluminescence (PL) measurements were conducted by a fluorescence spectrophotometer (Cary Eclipse, Agilent Technologies, Inc., Santa Clara, CA, USA) equipped with a Xe lamp. PL decay curves were detected using an EPL-405 nanosecond laser (Edinburgh Instruments Ltd., Livingston, Scotland, UK). The Fourier transform infrared (FTIR) analysis (KBr pellet method) was recorded using a Nicolet iS50 FTIR spectrometer (Thermo Fisher Scientific, Waltham, MA, USA). XPS spectra were recorded on a Thermo Fisher ESCALAB Xi+ spectrometer. The atomic force microscopy (AFM) images were analyzed by an atomic force microscope (MFP-3D-BIO, Asylum Research, Goleta, CA, USA). The characteristics of the fabricated LED devices were measured using one spectrograph of PR670 (Photo Research, New York, USA) with an analyzer system.

3. RESULTS AND DISCUSSION

A. Characterization of the $CsPbBr_3$ QDs

The detailed synthesis of $CsPbBr_3$-DA QDs can be found in the previous report [40]. The pristine $CsPbBr_3$-OA QDs were synthesized via the general hot-injection method using lead bromide and cesium oleate as precursors [16]. The synthesis scheme of the modified $CsPbBr_3$ QDs by using DA as a ligand to replace the regular OA ligand is schematically shown in Fig. 1(a). To confirm the successful synthesis of $CsPbBr_3$ QDs with a DA ligand, HRTEM, XRD, and FTIR spectra were recorded. Figure 1(b) shows the XRD patterns of the $CsPbBr_3$-OA QDs and $CsPbBr_3$-DA QDs. Both samples

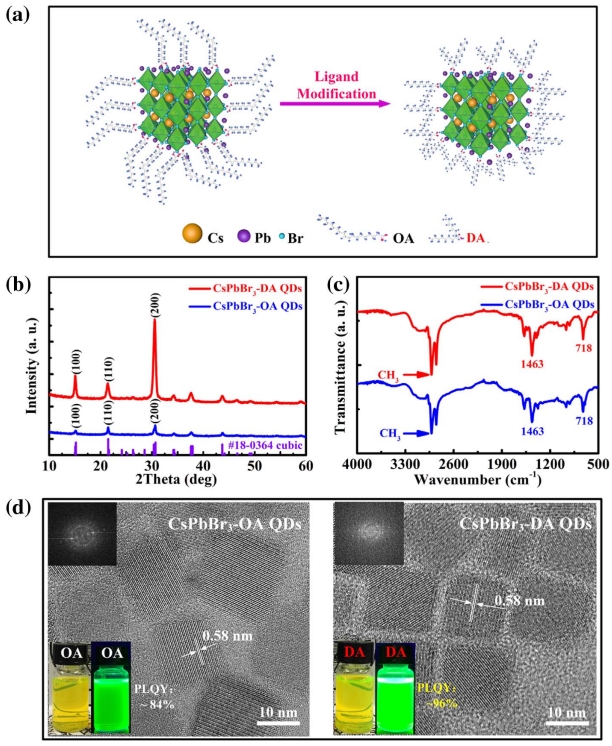

Fig. 1. (a) Schematic illustration of the surface in the $CsPbBr_3$ QDs with ligand modification process, (b) XRD patterns, (c) FTIR spectra, and (d) HRTEM images for $CsPbBr_3$ QDs.

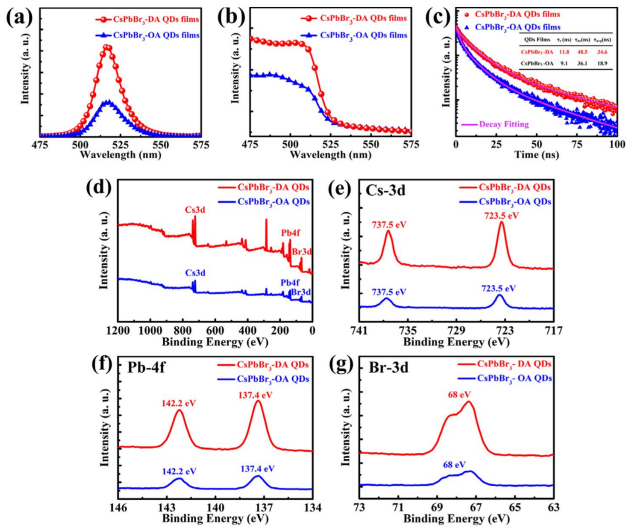

Fig. 2. (a) PL spectra, (b) absorption spectra, and (c) lifetime of the $CsPbBr_3$ QDs films. (d) XPS survey spectra of $CsPbBr_3$ QDs. (e) Cs-3d spectrum, (f) Pb-4f spectrum, and (g) Br-3d spectrum. All peaks were calibrated using C 1s (284.8 eV).

exhibit distinctive XRD peaks at $2\theta = 15.2°$, 21.5°, and 30.7°, which can be indexed to the (100), (110), and (200) planes of the $CsPbBr_3$ cubic phase [41–44], respectively. In addition, both XRD results of the $CsPbBr_3$ QDs are well indexed to the standard cubic $CsPbBr_3$ phase, without impure phases. It also can be seen that the crystallinities of the $CsPbBr_3$-DA QDs are notably higher than that of the $CsPbBr_3$-OA QDs. To investigate the surface ligand, the corresponding FTIR spectra were measured, as shown in Fig. 1(c). The peaks of CH_3 reveal the presence of the ligand on the surface of both $CsPbBr_3$ QDs. The peaks of 718 cm^{-1} are the peaks of -(CH_2)- which are the long-chain saturated hydrocarbons, further confirming the presence of the ligands. In particular, the peaks of 1463 cm^{-1} (-COOH-) for DA ligand and OA ligand imply that the $CsPbBr_3$ QDs are well capped with the OA/DA ligand after a cleaning process. HRTEM images reveal a cubic shape of the $CsPbBr_3$-OA and $CsPbBr_3$-DA QDs, with the average sizes of 11.66 nm and 12.44 nm, respectively [Fig. 1(d)]. In addition, the same lattice spacing of 0.58 nm for both $CsPbBr_3$ QDs is clearly observed from the HRTEM images [Fig. 1(d)], which is consistent with the (200) crystal plane of the cubic $CsPbBr_3$ structure. The HRTEM image also demonstrates that the $CsPbBr_3$ QDs have high crystallinity. Interestingly, the $CsPbBr_3$-DA QDs are found to exhibit a high PLQY of 96%, while the PLQY of $CsPbBr_3$-OA QDs is only 84% [left inset of Fig. 1(d)].

To better investigate the emitting properties of the $CsPbBr_3$ QDs, we further conducted the absorption and PL spectra of $CsPbBr_3$-OA and $CsPbBr_3$-DA QDs films. Figure 2(a) shows the PL peak of both QDs centered at around 516 nm, while their corresponding absorption peaks [Fig. 2(b)] appear at around 509 nm, indicating a slight Stokes shift [45]. It is important to note the FWHM values obtained from the PL spectra are 20 nm and 17 nm for $CsPbBr_3$-OA and $CsPbBr_3$-DA QDs, respectively, indicating high-purity green emission for both QDs. Moreover, the PL intensity of $CsPbBr_3$-DA QDs film is obviously enhanced under the same measurement condition. The time-resolved PL decay spectroscopy was used to study the lifetime of both QDs films. Biexponential behaviors are observed for both QDs films, indicating both QDs with the intact crystal structure and efficient radiative recombination. The inset table of Fig. 2(c) presents a summary of the comparison of the results for the two QDs consisting of a fast-decay component (τ_r), a slow-decay component (τ_{nr}), and the calculated average lifetime (τ_{avg}). Generally, the fast decay (τ_r) process originates from trap-assisted recombination, while the slow decay (τ_{nr}) process presents the free-charge carrier radiative recombination. $CsPbBr_3$-DA QDs film shows an average lifetime (τ_{avg}) of 34.6 ns, which is much longer than those of $CsPbBr_3$-OA QDs films (18.9 ns). The longer PL lifetime of $CsPbBr_3$-DA QDs films indicates lower trap state densities, which may be ascribed to a reduction of the nonradiative pathways. To further demonstrate the formation of two $CsPbBr_3$ QDs, the X-ray photoelectron spectroscopy (XPS) comparative analyses of $CsPbBr_3$-OA and $CsPbBr_3$-DA QDs were performed. The result reveals that both $CsPbBr_3$-OA QDs and $CsPbBr_3$-DA QDs are comprised of Cs, Pb, and Br elements, shown in Fig. 2(d). Both $CsPbBr_3$-OA and $CsPbBr_3$-DA QDs comprise all peaks labeled, which are consistent with the previous report [46]. The high-resolution XPS spectra corresponding to the core levels of Cs 3d (723.5 and 737.5 eV), Pb 4f (137.4 and 142.2 eV), and Br 3d (68 eV) are recorded [see Figs. 2(e), 2(f), and 2(g)]. The XPS results show no differences for both $CsPbBr_3$ QDs, implying that their

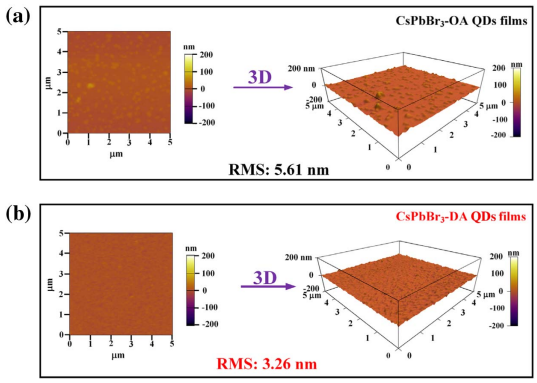

Fig. 3. AFM images of the (a) $CsPbBr_3$-OA and (b) $CsPbBr_3$-DA QDs films.

formation is well identified and both of them have been successfully synthesized.

The morphology of the $CsPbBr_3$ QDs films plays a very important role in achieving a bright green LED. To further probe the film qualities of the $CsPbBr_3$-OA QDs and $CsPbBr_3$-DA QDs films, we used AFM to characterize the morphology of $CsPbBr_3$-OA and $CsPbBr_3$-DA QDs films. Figure 3(a) shows that the $CsPbBr_3$-OA QDs film has a poor morphology with a high root mean square (RMS) surface average roughness of RMS ≈ 5.61 nm. However, after the DA ligand modification, $CsPbBr_3$-DA QDs perovskite films with better morphology are obtained and show a significant reduction in the RMS roughness; namely 3.26 nm for the $CsPbBr_3$-DA QDs films [see Fig. 3(b)].

B. Optical Properties of the Green LEDs

To demonstrate the green light emission conversion of QDs, the blue LEDs with an emission wavelength of 450 nm were used as an excitation source. The green LED devices were fabricated using $CsPbBr_3$-OA QDs and $CsPbBr_3$-DA QDs films as the active layer. We have designed a series of $CsPbBr_3$ QDs layers to explore the suitable quantity for the green LEDs and obtain nearly pure green emission. The emission spectrum of both $CsPbBr_3$ QDs as-coated LEDs has been recorded under room temperature. Figures 4(a) and 4(b) present the evolution of QDs coated on LEDs under the ambient conditions. Both of them undergo a change from blue to green light, indicating the $CsPbBr_3$ QDs layers have a favorable color conversion ability that converts blue light emission into a green one. Finally, the green light emission of the $CsPbBr_3$-OA QDs coated LEDs has a weak brightness, while the green LEDs with $CsPbBr_3$-DA QDs are much brighter with less QDs solution. Both $CsPbBr_3$-OA QDs and $CsPbBr_3$-DA QDs based LEDs have been explored under a constant driving current of 31.1 mA during the coating process. The spectrum variation in the processing of LEDs with different amounts of QDs is shown in Fig. 4(c). The two emission peaks of 450 nm and ~530 nm are contributed by the blue InGaN chips and $CsPbBr_3$-OA QDs, respectively. The quantity of the QDs solution addition is a key parameter for pure green LEDs. With an increase of the quantity of the QDs solution, the main blue emission peak of 450 nm reduces gradually, accompanied by an increase in the

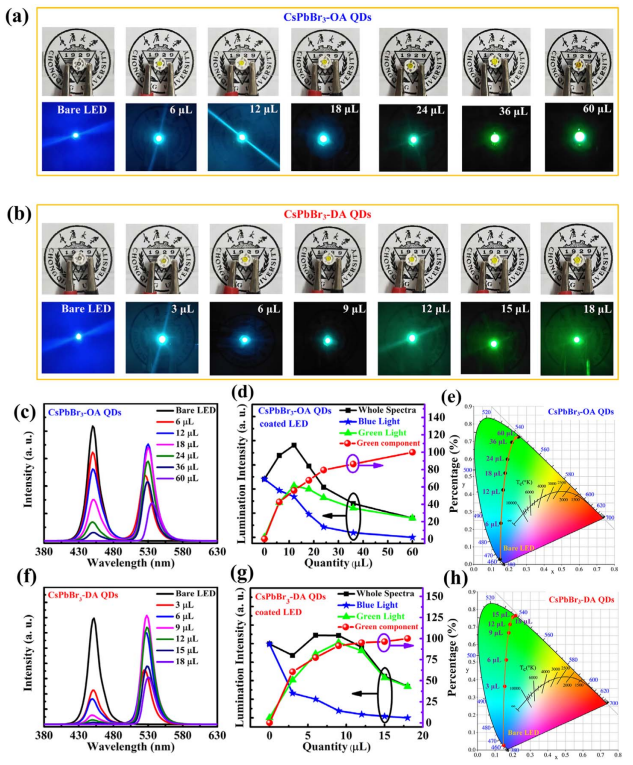

Fig. 4. (a) and (b) Evolution of $CsPbBr_3$ QDs coated on LED chips. The optical properties of (c)–(e) $CsPbBr_3$-OA QDs and (f)–(h) $CsPbBr_3$-DA QDs coated on LED chips. (c) and (f) Emission spectra, (d) and (g) green light purity analyses, and (e) and (h) behaviors of chromaticity coordinates with the addition of QDs solution.

green emission intensity. Finally, the blue emission peak of 450 nm almost disappears and the green emission peak of 530 nm becomes the main peak, implying that the QDs enable absorption of the emission of the blue InGaN chip completely and output the green emission intensively. It is obvious that the intensity of green emission increases to a maximum value with the $CsPbBr_3$-OA QDs up to 18 μL and then decreases with the addition of the QDs. Similarly, the addition of the $CsPbBr_3$-DA QDs onto blue LEDs causes a similar emission behavior. Compared to $CsPbBr_3$-OA QDs, a much smaller amount of the $CsPbBr_3$-DA QDs solution is required for pure green emission. In other words, the thickness of $CsPbBr_3$-DA QDs films is smaller than that of $CsPbBr_3$-OA QDs films due to the different amounts of the QDs solution required under the same experimental conditions [including the concentration (10 mg/mL), room temperature and air]. We ascribe this to the higher PLQY of $CsPbBr_3$-DA QDs solution.

In the presence of light-emitting components, the emission colors can be analyzed by a spectrum that shows the corresponding integrated intensity of the blue and green lights. As shown in Figs. 4(d) and 4(g), the percentage of $CsPbBr_3$-OA QDs based green emission increases with the amount of QDs. The energy transfer efficiency from blue to green light is presumed to be important for achieving a green LED and estimated by the ratio of the light integration. For example, it is calculated to be 79.4% at 24 μL. The figures reveal that the coated LEDs exhibit nearly pure green light when the coated

volume of the $CsPbBr_3$-OA QDs and the $CsPbBr_3$-DA QDs solutions reaches 60 μL and 18 μL, respectively. The smaller required amount of the $CsPbBr_3$-DA QDs solution can be attributed to the better optical properties of the $CsPbBr_3$-DA QDs compared to the $CsPbBr_3$-OA QDs. Furthermore, the intensity of the green light from LEDs based on $CsPbBr_3$-OA QDs increases slowly. We ascribe this phenomenon to the aggregation of the $CsPbBr_3$-OA QDs during the emitting process, while the $CsPbBr_3$-DA QDs might maintain better stability. We have confirmed that there is strong binding energy between the DA ligand and the QDs in our previous report; thus, the ligand could not lose easily during the emission process [40]. To investigate the quantification of the green emission light of the QDs coated LED, we have explored the light purity analyses on both $CsPbBr_3$-OA QDs and $CsPbBr_3$-DA QDs samples [Figs. 4(d) and 4(g)]. From blue to green, the color variation of the $CsPbBr_3$-OA samples is achieved by adding the QDs solution up to 60 μL, while the $CsPbBr_3$-DA samples change into the green region with only 18 μL. In terms of the calculation about light purity, the dominant wavelength plays an important role in the characterizing of the spectral light, and it can be speculated by the coordinates of the QDs coated LED and pure green light in the Commission Internationale Ed l'eclairage (CIE) diagram. Figures 4(e) and 4(h) show the CIE chromaticity coordinates of the spectrum, which reveals the process from blue to nearly pure green, with the increasing volume of the QDs solution. Finally, the chromaticity coordinates of the nearly pure green LEDs are reached at (0.2547, 0.7266) and (0.2086, 0.7635) for $CsPbBr_3$-OA and $CsPbBr_3$-DA QDs films, respectively. In addition, it is worth noting that the emission wavelength of the $CsPbBr_3$-OA QDs red shifted from 525 to 536 nm along with the addition of the solution, while the $CsPbBr_3$-DA QDs showed a small red shift. These red shifts can be ascribed to the QDs particles aggregation in solid-state, which is caused by the high temperature during the process.

C. Optoelectronic Properties

To further reveal the properties of the pure green emission, the emission spectra of the green LEDs under different currents have been measured. The voltage-current characteristics and the FWHM of both $CsPbBr_3$-OA QDs and $CsPbBr_3$-DA QDs coated on blue LEDs have been investigated. As shown in Figs. 5(a) and 5(d), the intensity of the pure green light increases gradually for both green LEDs along with the driving current increase from 0.4 mA to 64.7 mA. For $CsPbBr_3$-OA QDs coated LEDs, the FWHM varies from 17 to 20 nm and the emission peak position changes from 538 to 540 nm when the driving current increases from 0.4 to 64.7 mA. The changes could be attributed to the aggregation of the $CsPbBr_3$-OA QDs under high temperatures induced by the increasing current [Fig. 5(b)]. This phenomenon of thermally induced aggregation of $CsPbBr_3$ QDs has also been reported in other previous research [47–49]. In contrast, $CsPbBr_3$-DA QDs coated LEDs exhibit robust stabilities even under a high injection current (i.e., the FWHM remains 22 nm and the emission peak keeps the same position, respectively), as shown in Fig. 5(e). The corresponding CIE coordinates of the $CsPbBr_3$-OA QDs coated LEDs and $CsPbBr_3$-DA coated LEDs are (0.2547, 0.7266) and (0.2086, 0.7635), respectively, exhibiting no shift under the different injection current, as shown in Figs. 5(c) and 5(f). Notably, the power efficiency (43.6 lm/W) of $CsPbBr_3$-DA QDs coated LEDs is much higher than that of the $CsPbBr_3$-OA QDs coated LEDs (30.9 lm/W) under a 15.3 mA driving current. These results demonstrate that DA ligand modification for $CsPbBr_3$ QDs is a useful strategy to improve the performance of green LED devices.

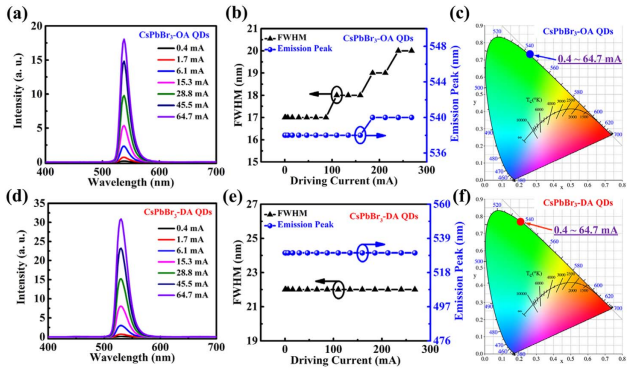

Fig. 5. Optical properties of QDs coated on blue LEDs. (a) and (d) Spectrum intensity, (b) and (e) FWHM, and (c) and (f) behaviors of chromaticity coordinates under different injection currents.

4. CONCLUSION

In summary, we have demonstrated that $CsPbBr_3$ QDs with DA ligand modification exhibit better properties than $CsPbBr_3$ QDs with a traditional OA ligand. Subsequently, we have fabricated green LEDs based on both $CsPbBr_3$-OA QDs and $CsPbBr_3$-DA QDs under the ambient conditions. Compared to $CsPbBr_3$-OA QDs coated LEDs, the LEDs coated by $CsPbBr_3$-DA QDs show higher purity, higher thermal stability, and stronger green light intensity. This work promotes the investigation of LEDs based on ligand-modified perovskite QDs.

Funding. National Natural Science Foundation of China (11974063); Fundamental Research Funds for the Central Universities (2019CDJGFGD001); Graduate Scientific Research and Innovation Foundation of Chongqing (CYB19036).

Disclosures. The authors declare that there are no conflicts of interest related to this paper.

REFERENCES

1. J. Cho, J. H. Park, J. K. Kim, and E. F. Schubert, "White light-emitting diodes: history, progress, and future," Laser Photon. Rev. **11**, 1600147 (2017).
2. M. R. Krames, O. B. Shchekin, R. Mueller-Mach, G. Mueller, L. Zhou, G. Harbers, and M. G. Craford, "Status and future of high-power light-emitting diodes for solid-state lighting," J. Display Technol. **3**, 160–175 (2007).
3. S. Nakamura, M. Senoh, N. Iwasa, and S.-I. Nagahama, "High-brightness InGaN blue, green and yellow light-emitting diodes

with quantum well structures," Jpn. J. Appl. Phys. **34**, L797-L799 (1995).
4. A. Liu, A. Khanna, P. S. Dutta, and M. Shur, "Red-blue-green solid state light sources using a narrow line-width green phosphor," Opt. Express **23**, A309–A315 (2015).
5. T. Langer, A. Kruse, F. A. Ketzer, A. Schwiegel, L. Hoffmann, H. Jönen, H. Bremers, U. Rossow, and A. Hangleiter, "Origin of the green gap: increasing nonradiative recombination in indium-rich GaInN/GaN quantum well structures," Phys. Status Solidi C **8**, 2170–2172 (2011).
6. Y. Tong, E. Bladt, M. F. Aygüler, A. Manzi, K. Z. Milowska, V. A. Hintermayr, P. Docampo, S. Bals, A. S. Urban, L. Polavarapu, and J. Feldmann, "Highly luminescent cesium lead halide perovskite nanocrystals with tunable composition and thickness by ultrasonication," Angew. Chem. Int. Ed. **55**, 13887–13892 (2016).
7. I. Lignos, L. Protesescu, D. B. Emiroglu, R. Maceiczyk, S. Schneider, M. V. Kovalenko, and A. J. deMello, "Unveiling the shape evolution and halide-ion-segregation in blue-emitting formamidinium lead halide perovskite nanocrystals using an automated microfluidic platform," Nano Lett. **18**, 1246–1252 (2018).
8. F. Nippert, S. Y. Karpov, G. Callsen, B. Galler, T. Kure, C. Nenstiel, M. R. Wagner, M. Straßburg, H.-J. Lugauer, and A. Hoffmann, "Temperature-dependent recombination coefficients in InGaN light-emitting diodes: hole localization, Auger processes, and the green gap," Appl. Phys. Lett. **109**, 161103 (2016).
9. S. Saito, R. Hashimoto, J. Hwang, and S. Nunoue, "InGaN light-emitting diodes ONC-face sapphire substrates in green gap spectral range," Appl. Phys. Express **6**, 111004 (2013).
10. D. Alexander, K. Thomas, S. Sisira, G. Vimal, K. P. Mani, P. R. Biju, N. V. Unnikrishnan, M. A. Ittyachen, and C. Joseph, "Photoluminescence properties of fully concentrated terbium oxalate: a novel efficient green emitting phosphor," Mater. Lett. **189**, 160–163 (2017).
11. M. Zhao, H. Liao, L. Ning, Q. Zhang, Q. Liu, and Z. Xia, "Next-generation narrow-band green-emitting $RbLi(Li_3SiO_4)_2:Eu^{2+}$ phosphor for backlight display application," Adv. Mater. **30**, 1802489 (2018).
12. Y. Liu, J. Zhang, C. Zhang, J. Jiang, and H. Jiang, "High efficiency green phosphor $Ba_9Lu_2Si_6O_{24}:Tb^{3+}$: visible quantum cutting via cross-relaxation energy transfers," J. Phys. Chem. C **120**, 2362–2370 (2016).
13. Y. Xiao, Z. Hao, L. Zhang, X. Zhang, G.-H. Pan, H. Wu, H. Wu, Y. Luo, and J. Zhang, "An efficient green phosphor of Ce^{3+} and Tb^{3+}-codoped $Ba_2Lu_5B_5O_{17}$ and a model for elucidating the high thermal stability of the green emission," J. Mater. Chem. C **6**, 5984–5991 (2018).
14. Z. Yang, D. Xu, J. Sun, J. Du, and X. Gao, "Luminescence properties and energy transfer investigations of $Sr_3Lu(PO_4)_3:Ce^{3+}$, Tb^{3+} phosphors," Mater. Sci. Eng. B **211**, 13–19 (2016).
15. H. Zhou, Q. Wang, M. Jiang, X. Jiang, and Y. Jin, "A novel green-emitting phosphor $Ba_2Gd_2Si_4O_{13}:Eu^{2+}$ for near UV-pumped light-emitting diodes," Dalton Trans. **44**, 13962–13968 (2015).
16. L. Protesescu, S. Yakunin, M. I. Bodnarchuk, F. Krieg, R. Caputo, C. H. Hendon, R. X. Yang, A. Walsh, and M. V. Kovalenko, "Nanocrystals of cesium lead halide perovskites ($CsPbX_3$, X = Cl, Br, and I): novel optoelectronic materials showing bright emission with wide color gamut," Nano Lett. **15**, 3692–3696 (2015).
17. J. De Roo, M. Ibáñez, P. Geiregat, G. Nedelcu, W. Walravens, J. Maes, J. C. Martins, I. Van Driessche, M. V. Kovalenko, and Z. Hens, "Highly dynamic ligand binding and light absorption coefficient of cesium lead bromide perovskite nanocrystals," ACS Nano **10**, 2071–2081 (2016).
18. S. Yakunin, L. Protesescu, F. Krieg, M. I. Bodnarchuk, G. Nedelcu, M. Humer, G. De Luca, M. Fiebig, W. Heiss, and M. V. Kovalenko, "Low-threshold amplified spontaneous emission and lasing from colloidal nanocrystals of caesium lead halide perovskites," Nat. Commun. **6**, 8056 (2015).
19. A. Swarnkar, R. Chulliyil, V. K. Ravi, M. Irfanullah, A. Chowdhury, and A. Nag, "Colloidal $CsPbBr_3$ perovskite nanocrystals: luminescence beyond traditional quantum dots," Angew. Chem. Int. Ed. **54**, 15424–15428 (2015).
20. J. Li, H. Dong, B. Xu, S. Zhang, Z. Cai, J. Wang, and L. Zhang, "$CsPbBr_3$ perovskite quantum dots: saturable absorption properties and passively *Q*-switched visible lasers," Photon. Res. **5**, 457–460 (2017).
21. Y. Zhang, H. Zhu, T. Huang, Z. Song, and S. Ruan, "Radiation-pressure-induced photoluminescence enhancement of all-inorganic perovskite $CsPbBr_3$ quantum dots," Photon. Res. **7**, 837–846 (2019).
22. X. Li, Y. Wu, S. Zhang, B. Cai, Y. Gu, J. Song, and H. Zeng, "$CsPbX_3$ quantum dots for lighting and displays: room-temperature synthesis, photoluminescence superiorities, underlying origins and white light-emitting diodes," Adv. Funct. Mater. **26**, 2435–2445 (2016).
23. S. D. Stranks and H. J. Snaith, "Metal-halide perovskites for photovoltaic and light-emitting devices," Nat. Nanotechnology **10**, 391–402 (2015).
24. J. Pan, S. P. Sarmah, B. Murali, I. Dursun, W. Peng, M. R. Parida, J. Liu, L. Sinatra, N. Alyami, C. Zhao, E. Alarousu, T. K. Ng, B. S. Ooi, O. M. Bakr, and O. F. Mohammed, "Air-stable surface-passivated perovskite quantum dots for ultra-robust, single- and two-photon-induced amplified spontaneous emission," J. Phys. Chem. Lett. **6**, 5027–5033 (2015).
25. G. Nedelcu, L. Protesescu, S. Yakunin, M. I. Bodnarchuk, M. J. Grotevent, and M. V. Kovalenko, "Fast anion-exchange in highly luminescent nanocrystals of cesium lead halide perovskites ($CsPbX_3$, X = Cl, Br, I)," Nano Lett. **15**, 5635–5640 (2015).
26. K. Wu, G. Liang, Q. Shang, Y. Ren, D. Kong, and T. Lian, "Ultrafast interfacial electron and hole transfer from $CsPbBr_3$ perovskite quantum dots," J. Am. Chem. Soc. **137**, 12792–12795 (2015).
27. B. R. Sutherland and E. H. Sargent, "Perovskite photonic sources," Nat. Photonics **10**, 295–302 (2016).
28. I. Dursun, C. Shen, M. R. Parida, J. Pan, S. P. Sarmah, D. Priante, N. Alyami, J. Liu, M. I. Saidaminov, M. S. Alias, A. L. Abdelhady, T. K. Ng, O. F. Mohammed, B. S. Ooi, and O. M. Bakr, "Perovskite nanocrystals as a color converter for visible light communication," ACS Photon. **3**, 1150–1156 (2016).
29. C. H. Kang, I. Dursun, G. Liu, L. Sinatra, X. Sun, M. Kong, J. Pan, P. Maity, E.-N. Ooi, T. K. Ng, O. F. Mohammed, O. M. Bakr, and B. S. Ooi, "High-speed colour-converting photodetector with all-inorganic $CsPbBr_3$ perovskite nanocrystals for ultraviolet light communication," Light Sci. Appl. **8**, 94 (2019).
30. F. Zhang, J. Song, B. Han, T. Fang, J. Li, and H. Zeng, "High-efficiency pure-color inorganic halide perovskite emitters for ultra-high-definition displays: progress for backlighting displays and electrically driven devices," Small Methods **2**, 1700382 (2018).
31. S. A. Veldhuis, P. P. Boix, N. Yantara, M. Li, T. C. Sum, N. Mathews, and S. G. Mhaisalkar, "Perovskite materials for light-emitting diodes and lasers," Adv. Mater. **28**, 6804–6834 (2016).
32. H. Guan, S. Zhao, H. Wang, D. Yan, M. Wang, and Z. Zang, "Room temperature synthesis of stable single silica-coated $CsPbBr_3$ quantum dots combining tunable red emission of Ag–In–Zn–S for high-CRI white light-emitting diodes," Nano Energy **67**, 104279 (2020).
33. C. Li, Z. Zang, W. Chen, Z. Hu, X. Tang, W. Hu, K. Sun, X. Liu, and W. Chen, "Highly pure green light emission of perovskite $CsPbBr_3$ quantum dots and their application for green light-emitting diodes," Opt. Express **24**, 15071–15078 (2016).
34. J. Song, J. Li, X. Li, L. Xu, Y. Dong, and H. Zeng, "Quantum dot light-emitting diodes based on inorganic perovskite cesium lead halides ($CsPbX_3$)," Adv. Mater. **27**, 7162–7167 (2015).
35. Z. Ning, O. Voznyy, J. Pan, S. Hoogland, V. Adinolfi, J. Xu, M. Li, A. R. Kirmani, J.-P. Sun, J. Minor, K. W. Kemp, H. Dong, L. Rollny, A. Labelle, G. Carey, B. Sutherland, I. Hill, A. Amassian, H. Liu, J. Tang, O. M. Bakr, and E. H. Sargent, "Air-stable n-type colloidal quantum dot solids," Nat. Mater. **13**, 822–828 (2014).
36. J. Pan, L. N. Quan, Y. Zhao, W. Peng, B. Murali, S. P. Sarmah, M. Yuan, L. Sinatra, N. M. Alyami, J. Liu, E. Yassitepe, Z. Yang, O. Voznyy, R. Comin, M. N. Hedhili, O. F. Mohammed, Z. H. Lu, D. H. Kim, E. H. Sargent, and O. M. Bakr, "Highly efficient perovskite-quantum-dot light-emitting diodes by surface engineering," Adv. Mater. **28**, 8718–8725 (2016).
37. X. Zhang, B. Xu, J. Zhang, Y. Gao, Y. Zheng, K. Wang, and X. W. Sun, "All-inorganic perovskite nanocrystals for high-efficiency light emitting diodes: dual-phase $CsPbBr_3$-$CsPb_2Br_5$ composites," Adv. Funct. Mater. **26**, 4595–4600 (2016).

38. C. Wu, Y. Zou, T. Wu, M. Ban, V. Pecunia, Y. Han, Q. Liu, T. Song, S. Duhm, and B. Sun, "Improved performance and stability of all-inorganic perovskite light-emitting diodes by antisolvent vapor treatment," Adv. Funct. Mater. **27**, 1700338 (2017).
39. H. Wu, Y. Zhang, M. Lu, X. Zhang, C. Sun, T. Zhang, V. L. Colvin, and W. W. Yu, "Surface ligand modification of cesium lead bromide nanocrystals for improved light-emitting performance," Nanoscale **10**, 4173–4178 (2018).
40. D. Yan, T. Shi, Z. Zang, T. Zhou, Z. Liu, Z. Zhang, J. Du, Y. Leng, and X. Tang, "Ultrastable $CsPbBr_3$ perovskite quantum dot and their enhanced amplified spontaneous emission by surface ligand modification," Small **15**, 1901173 (2019).
41. L. Xu, J. Li, T. Fang, Y. Zhao, S. Yuan, Y. Dong, and J. Song, "Synthesis of stable and phase-adjustable $CsPbBr_3@Cs_4PbBr_6$ nanocrystals via novel anion-cation reactions," Nanoscale Adv. **1**, 980–988 (2019).
42. C. Chen, L. Zhang, T. Shi, G. Liao, and Z. Tang, "Controllable synthesis of all inorganic lead halide perovskite nanocrystals with various appearances in multiligand reaction system," Nanomaterials (Basel) **9**, 1751 (2019).
43. Y. Chang, Y. J. Yoon, G. Li, E. Xu, S. Yu, C.-H. Lu, Z. Wang, Y. He, C. H. Lin, B. K. Wagner, V. V. Tsukruk, Z. Kang, N. Thadhani, Y. Jiang, and Z. Lin, "All-inorganic perovskite nanocrystals with a stellar set of stabilities and their use in white light-emitting diodes," ACS. Appl. Mater. Interface **10**, 37267–37276 (2018).
44. Z. Liu, B. Sun, X. Liu, J. Han, H. Ye, T. Shi, Z. Tang, and G. Liao, "Efficient carbon-based $CsPbBr_3$ inorganic perovskite solar cells by using Cu-phthalocyanine as hole transport material," Nano-Micro Lett. **10**, 34 (2018).
45. M. C. Brennan, J. E. Herr, T. S. Nguyen-Beck, J. Zinna, S. Draguta, S. Rouvimov, J. Parkhill, and M. Kuno, "Origin of the size-dependent Stokes shift in $CsPbBr_3$ perovskite nanocrystals," J. Am. Chem. Soc. **139**, 12201–12208 (2017).
46. M. Liu, G. Zhong, Y. Yin, J. Miao, K. Li, C. Wang, X. Xu, C. Shen, and H. Meng, "Aluminum-doped cesium lead bromide perovskite nanocrystals with stable blue photoluminescence used for display backlight," Adv. Sci. **4**, 1700335 (2017).
47. I. Lignos, S. Stavrakis, G. Nedelcu, L. Protesescu, A. J. deMello, and M. V. Kovalenko, "Synthesis of cesium lead halide perovskite nanocrystals in a droplet-based microfluidic platform: fast parametric space mapping," Nano Lett. **16**, 1869–1877 (2016).
48. B. T. Diroll, G. Nedelcu, M. V. Kovalenko, and R. D. Schaller, "High-temperature photoluminescence of $CsPbX_3$ (X = Cl, Br, I) nanocrystals," Adv. Funct. Mater. **27**, 1606750 (2017).
49. S. Yuan, Z.-K. Wang, M.-P. Zhuo, Q.-S. Tian, Y. Jin, and L.-S. Liao, "Self-assembled high quality $CsPbBr_3$ quantum dot films toward highly efficient light-emitting diodes," ACS Nano **12**, 9541–9548 (2018).